International Journal on Magnetic Particle Imaging
Vol 8, No 1, Suppl 1, Article ID 2203015, 4 Pages

Infinite Science Publishing

Proceedings Article

Efficient 3D Drive-Field Characterization for Magnetic Particle Imaging Systems

Florian Thieben [1,2,*] · Marija Boberg [1,2,*] · Matthias Graeser [1,2,3,4] · Tobias Knopp [1,2]

[1]Section for Biomedical Imaging, University Medical Center Hamburg-Eppendorf, Hamburg, Germany
[2]Institute for Biomedical Imaging, Hamburg University of Technology, Hamburg, Germany
[3]Fraunhofer Research Institute for Individualized and Cell-based Medicine, Lübeck, Germany
[4]Institute of Medical Engineering, University of Lübeck, Lübeck, Germany
*Corresponding author, email: f.thieben@uke.de, m.boberg@uke.de

Abstract

Magnetic particle imaging uses time-dependent drive fields for signal generation, which are designed to be homogeneous in order to achieve a similar image quality all over the volume of interest. In practice, the fields are not exactly homogeneous and in turn a precise knowledge of the spatial field profile is necessary when using a model-based reconstruction approach. In this work, we propose an efficient method for the measurement and a compact representation of the drive fields using a small three-axis coil sensor and solid harmonics.

I. Introduction

In magnetic particle imaging (MPI), signal generation and encoding is achieved by the superposition of static and dynamic magnetic fields. For system modeling [1] and in particular model-based image reconstruction [2], precise knowledge of the magnetic fields is of great importance. In general, the fields differ from the ideal case, i.e. the selection field is not perfectly linear and the drive field is not perfectly homogeneous in space. A simulation of the magnetic fields is possible but requires precise knowledge of all system components. An alternative approach is the measurement of the fields using a robot and a field sensor [3]. For static fields, this is usually done by using a Hall-effect sensor, since an inductive measurement would not generate any signal [4].

In this work, we focus on the measurement of the drive fields, which are measured inductively using a small three-axis coil sensor. Our method requires only few measurements and allows measuring the magnetic fields at the frequency applied during the actual MPI experiment. In this way, eddy current induced field attenuation caused by shielding components is also taken into account.

II. Methods and Materials

The proposed method consists of three steps: Field measurement, field calculation, and field representation. The voltage signals induced in a small three-axis coil sensor are measured at several positions and converted into magnetic-field values exploiting Faraday's law of induction. Solid harmonic expansions are used for the representation of the drive fields. They offer a compact magnetic field representation so that only a few measurement points on a sphere (spherical t-design) are required for an accurate model of the spatially dependent drive field. In the following, each of the three steps is described in more detail.

II.I. Field Measurement

The three-axis coil sensor used for the measurements of the alternating magnetic fields is shown in Fig. 1. Each coil c_i, $i \in \{x, y, z\}$, has $N_i \in \mathbb{N}$ windings with radius $r_i \in \mathbb{R}^{>0}$ and surface area $A_i = \pi r_i^2$. The sensor is connected to a data acquisition (DAQ) system via a voltage divider. The voltage divider has a transfer function $\tilde{R} = \frac{R_1 + R_{\mathrm{DAQ}} + R_2}{R_{\mathrm{DAQ}}} \in \mathbb{R}$ (Fig. 1, blue framed) and serves as a matching circuit for the DAQ system. In this work, the voltages induced by the alternating magnetic fields are measured using the DAQ system at the same channels

10.18416/ijmpi.2022.2203015

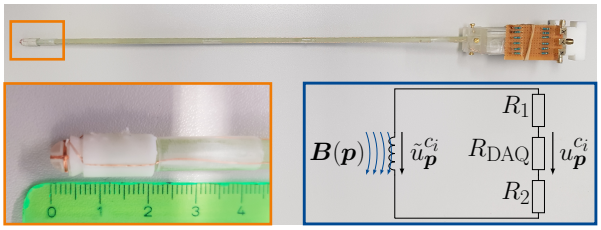

Figure 1: On top the three-axis coil sensor is depicted. In the orange-framed box a magnified view of the three orthogonal coils is shown with a scale. In the blue-framed box a simplified electrical circuit of one dimension of the sensor is sketched. The drive field B induces a voltage $\tilde{u}^{c_i}$ in each coil. The resistors R_1, R_2 and R_{DAQ} set up a voltage divider to reduce the voltage drop u^{c_i} across R_{DAQ} that is measured with the DAQ system.

that are otherwise used for MPI signal reception. In this way a sample-accurate digitization with a high bandwidth above 1 MHz can be performed. The three-axis coil sensor with the voltage divider circuit is mounted on a robot that is used to move the sensor in space. At each t-design position $\boldsymbol{p} \in \mathbb{R}^3$, one 3D drive field cycle is applied and the voltage signal $u_{\boldsymbol{p}}^{c_i} : \mathbb{R} \to \mathbb{R}$ is measured for each coil.

II.II. Field Calculation

A section of an exemplary voltage signal measured with coil c_x at the first t-design position $\boldsymbol{p}_1$ is shown at the top of Fig. 2. Since each drive field has its own unique excitation frequency, the voltage signal is Fourier transformed yielding the signal $\hat{u}_{\boldsymbol{p}}^{c_i} : \mathbb{R} \to \mathbb{C}$. In Fourier space, the signal at the three excitation frequencies f_j, $j \in \{x, y, z\}$ can be clearly detected as it is shown in the central plot of Fig. 2. For each excitation frequency the magnetic flux density $\boldsymbol{B}_{f_j} : \mathbb{R}^3 \to \mathbb{R}^3$ is calculated by

$$B_{f_j}^{i}(\boldsymbol{p}) = \sigma\left(\hat{u}_{\boldsymbol{p}}^{c_i}(f_i), \hat{u}_{\boldsymbol{p}}^{c_i}(f_j)\right) \frac{1}{2\pi f_j N_i A_i} \underbrace{\tilde{R}\left|\hat{u}_{\boldsymbol{p}}^{c_i}(f_j)\right|}_{=\hat{u}_{\boldsymbol{p}}^{c_i}(f_j)} \tag{1}$$

where

$$\sigma : \mathbb{C} \times \mathbb{C} \to \{-1, 1\},$$
$$\sigma(\hat{u}_1, \hat{u}_2) = \begin{cases} 1 & \text{if } \arg(\hat{u}_1) \approx \arg(\hat{u}_2) \\ -1 & \text{else} \end{cases}$$

indicates the sign of the magnetic field, respectively the directions of the field vectors, which depends on the phase relation of the Fourier transformed signals. The third plot in Fig. 2 shows exemplary phases of the signal measured with coil c_x for several t-design positions. Here, $\sigma\left(\hat{u}_{\boldsymbol{p}}^{c_x}(f_x), \hat{u}_{\boldsymbol{p}}^{c_x}(f_j)\right) = 1$ if $\arg(\hat{u}_{\boldsymbol{p}}^{c_x}(f_j))$ lies within the light blue area, which compensates measurement uncertainties.

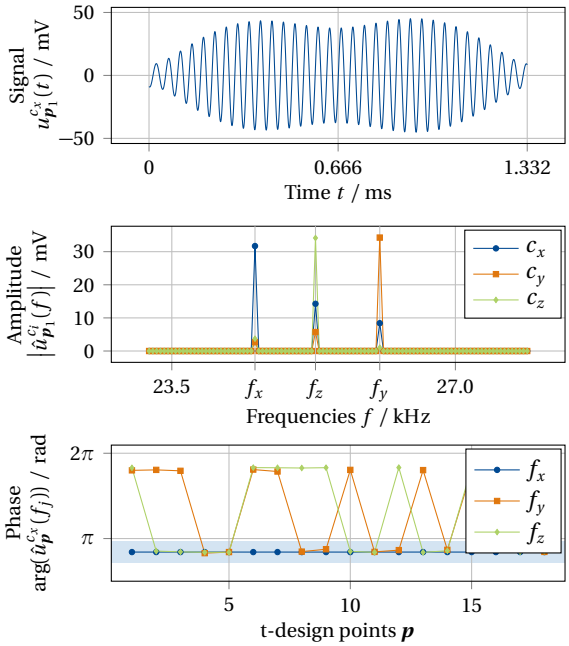

Figure 2: On top, a section of an exemplary voltage signal $u_{\boldsymbol{p}_1}^{c_x}(t)$ of a 21.54 ms 3D drive field induced in coil c_x at t-design position $\boldsymbol{p}_1$ is visualized. In the middle, a part of the Fourier transformed voltages $\hat{u}_{\boldsymbol{p}_1}^{c_i}(f)$ are shown. Due to the unique excitation frequencies f_x, f_y and f_z, the signal can be separated into the voltages $\hat{u}_{\boldsymbol{p}}^{c_i}(f_j)$ corresponding to the drive field $\boldsymbol{B}_{f_j}$. At the bottom, the phases of $\hat{u}_{\boldsymbol{p}}^{c_x}(f_j)$ are shown for a set of t-design positions. If the phase of $\hat{u}_{\boldsymbol{p}}^{c_x}(f_j)$ lies within a certain area around $\hat{u}_{\boldsymbol{p}}^{c_x}(f_x)$ (marked in light blue) the resulting magnetic flux density has a positive sign.

II.III. Field Representation

Finally, the measured field values are used to calculate the coefficients $\boldsymbol{\gamma}_{l,m}^{f_j} \in \mathbb{R}^3$ of the solid harmonic expansion for each drive field

$$\boldsymbol{B}_{f_j}(\boldsymbol{r}) = \sum_{l=0}^{L} \sum_{m=-l}^{l} \boldsymbol{\gamma}_{l,m}^{f_j} Z_l^m(\boldsymbol{r})$$

where $Z_l^m : \mathbb{R}^3 \to \mathbb{R}$ are the real normalized solid harmonics. The coefficients are calculated by the inner product of the measured drive field $\boldsymbol{B}_{f_j}(\boldsymbol{p})$ and $Z_l^m(\boldsymbol{p})$. The spherical t-design is used for sampling the sphere with radius $r_s \in \mathbb{R}^{>0}$. Utilizing the t-design requires only a few nodes for an exact integration, which is needed for the inner product. For calculating the coefficients up to degree $l = L$ a $2L$-design is required. [3]

III. Experiments

The developed method is used to characterize the drive fields of the pre-clinical MPI system 25/20FF (Bruker Corporation, Ettlingen, Germany). The MPI system features three excitation frequencies $f_x = \frac{2.5}{102}$ MHz, $f_y = \frac{2.5}{96}$ MHz, and $f_z = \frac{2.5}{99}$ MHz and is characterized at a drive-field

10.18416/ijmpi.2022.2203015

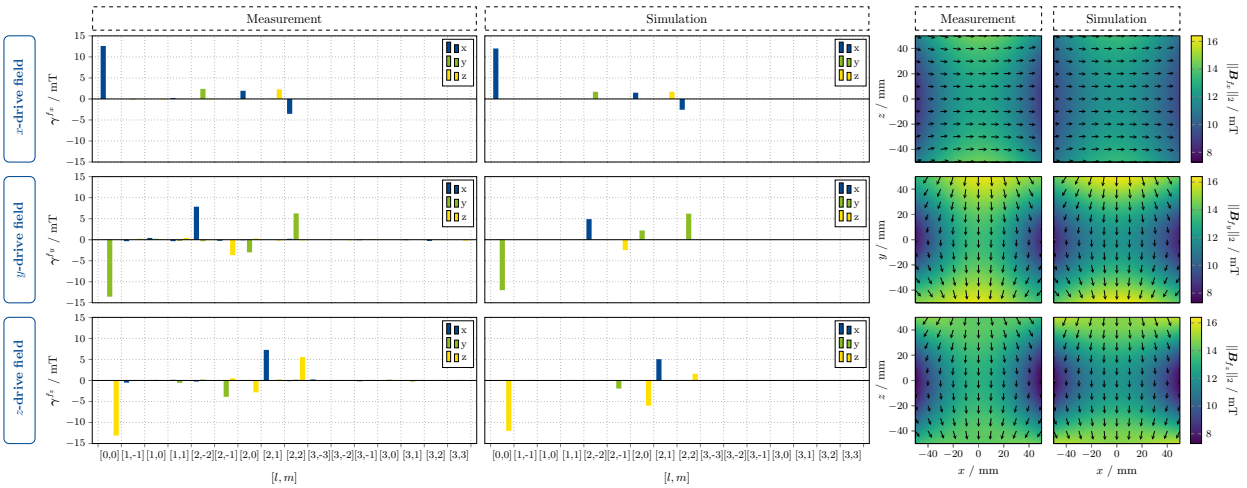

Figure 3: Visualization of the drive fields. On the left, the calculated solid coefficients are shown for each measured drive field. Next to it, the simulated coefficients are shown. The resulting magnetic field profile is depicted on the right, for both the measured and simulated case.

amplitude of 12 mT in x-, y-, and z-directions. The induction-based field sensor shown in Fig. 1 consists of three orthogonal coils arranged around the same center and each with a radius of $r = 2.5$ mm and 10 windings. The component and manufacturing tolerances of the sensor result in a maximum field tolerance of ±8 %. The sensor is mounted on a robot (isel Germany AG, Eichenzell, Germany) and connected to the DAQ system of the MPI scanner. The voltage divider of the electronic circuit has a transfer function of $\tilde{R} = 12.52$.

Field measurements with the three-axis coil sensor are performed at 36 positions of an 8-design laying on a sphere with radius $r_s = 50$ mm. This offers coefficients up to degree $L = 4$. To improve the signal quality, 100 drive-field cycles are acquired and averaged before field calculation, which leads to a total measurement time of 2 min. For validation, the measured coefficients of the solid harmonic expansion are compared to the coefficients of the drive field simulated with the Biot-Savart law and normalized to 12 mT. However, the simulation excludes eddy current losses within the shielding and coil coupling.

The measurement data is acquired using Bruker's system-matrix method and further data handling is done with the `MPIFiles.jl` [5] and `SphericalHarmonicExpansions.jl` [6] packages.

IV. Results and Discussion

Fig. 3 shows the measured and simulated coefficients of the solid harmonic expansion. Only small deviations between the coefficients can be observed. On the right hand side of Fig. 3, the measured and simulated magnetic field profiles with their imperfections are shown. The coefficients for $l \geq 1$ visualize the imperfections and show that they also occur orthogonal to the actual drive-field direction. Thus, the drive fields are not exactly orthogonal in each position, which is already visible in the measured data in Fig. 2. It is important to note that the solid harmonic expansion provides accurate results only within the measured sphere, which was chosen as large as possible inside the scanner bore. With the developed method the absolute value of the drive-field amplitude in the center is equal to 12.59, 13.55, and 13.10 mT in x-, y- and z-direction. The deviation to the set value of 12 mT exceeds the calculated tolerance of 8 % from the error propagation. Currently, the measured fields are only specified via the forward model (1). For higher accuracy, a scalar calibration factor can be determined via a measurement in a defined setup with Helmholtz coils [7] and multiplied to Eq. (1).

V. Conclusion

We presented an efficient method for spatially dependent 3D drive-field characterization with only 36 measurements without prior knowledge of the system. The gained knowledge of the drive field is crucial to improve model-based reconstruction methods [2, 8] and hybrid calibration methods [9]. Additionally it allows for calculating the feed-through signal coupling into receive coils, which can be used to design the cancellation coils within a gradiometric receiver. In order to gain more certainty about the sensor accuracy, a calibration within a known drive field should be performed.

Author's statement

Research funding: The authors thankfully acknowledge the financial support by the German Research Foundation (DFG, grant number KN 1108/7-1 and GR 5287/2-1).
Conflict of interest: Authors state no conflict of interest.

References

[1] H. Albers, T. Knopp, M. Möddel, M. Boberg, and T. Kluth. Modeling the magnetization dynamics for large ensembles of immobilized magnetic nanoparticles in multi-dimensional magnetic particle imaging. *Journal of Magnetism and Magnetic Materials*, 543:168534, 2022, doi:10.1016/j.jmmm.2021.168534.

[2] T. Kluth, P. Szwargulski, and T. Knopp. Towards accurate modeling of the multidimensional magnetic particle imaging physics. *New journal of physics*, 21(10):103032, 2019.

[3] M. Boberg, T. Knopp, and M. Möddel. Analysis and comparison of magnetic fields in MPI using spherical harmonic expansions. *Book of Abstracts IWMPI*, 2018.

[4] A. Weber, Imperfektionen bei magnetic particle imaging, PhD thesis, University of Lübeck, 2017,

[5] T. Knopp, M. Möddel, F. Griese, F. Werner, P. Szwargulski, N. Gdaniec, and M. Boberg. MPIFiles.jl: a julia package for magnetic particle imaging files. *Journal of Open Source Software*, 4(38):1331, 2019, doi:10.21105/joss.01331.

[6] SphericalHarmonicExpansions.jl: A Julia package to handle spherical harmonic functions, https://github.com/hofmannmartin/SphericalHarmonicExpansions.jl, Version: 0.1.

[7] E. Bronaugh, Helmholtz coils for calibration of probes and sensors: Limits of magnetic field accuracy and uniformity, in *Proceedings of International Symposium on Electromagnetic Compatibility*, 72–76, 1995. doi:10.1109/ISEMC.1995.523521.

[8] M. Boberg, T. Knopp, and M. Möddel. Reducing displacement artifacts by warping system matrices in efficient joint multi-patch magnetic particle imaging. *International Journal on Magnetic Particle Imaging*, 6(2 Suppl 1), 2020, doi:10.18416/IJMPI.2020.2009030.

[9] A. von Gladiss, M. Graeser, A. Cordes, A. C. Bakenecker, A. Behrends, X. Chen, and T. M. Buzug. Investigating spatial resolution, field sequences and image reconstruction strategies using hybrid phantoms in MPI. *International Journal on Magnetic Particle Imaging*, 6(1), 2020.